Fusion Engineering and Design 123 (2017) 612–615

Contents lists available at ScienceDirect

Fusion Engineering and Design

journal homepage: www.elsevier.com/locate/fusengdes

3D electromagnetic analysis of the MHD control system in RFX-mod upgrade

Paolo Bettini [a,b,*], Piergiorgio Alotto [b], Tommaso Bolzonella [a], Roberto Cavazzana [a], Luca Grando [a], Giuseppe Marchiori [a], Lionello Marrelli [a], Leonardo Pigatto [a], Ruben Specogna [c], Paolo Zanca [a]

[a] Consorzio RFX, C.so Stati Uniti 4, 35127 Padova, Italy
[b] University of Padova, Department of Industrial Engineering, 35131 Padova, Italy
[c] University of Udine, Polytechnic Department of Engineering and Architecture, 33100 Udine, Italy

HIGHLIGHTS

- Fast and efficient algorithms for the solution of 3D eddy current problems.
- Eddy current problems in complex magnetic confinement fusion devices.
- Numerical studies aiming at the upgrade of the MHD control system of RFX-mod.

ARTICLE INFO

Article history:
Received 3 October 2016
Received in revised form 16 February 2017
Accepted 24 February 2017
Available online 11 March 2017

Keywords:
RFXmod
Integral formulation
Eddy currents
Thin shields
MHD
Active feedback control

ABSTRACT

RFX-mod is a device equipped with a state-of-the-art system for active control of MHD instabilities, which consists of 192 saddle coils and 192 radial field sensors. In order to further extend its operational space an upgrade of its magnetic front-end is now being studied. In this paper we focus on the implementation of fast and efficient algorithms for the 3D electromagnetic analysis of the effect of the designed magnetic front-end on the MHD control system in RFX-mod2, in the presence of complex conducting structures surrounding the plasma.

1. Introduction

In modern experiments, excellent results have been achieved in the stabilisation of both axisymmetric vertical instabilities, that can occur in elongated plasmas, and non-axisymmetric modes, that tend to deform the plasma boundary. In this paper, we focus on RFX-mod, a medium size toroidal device ($R = 2$ m, $a = 0.459$ m) that has been operating since 2004 [1,2]. It is equipped with a state-of-the-art system for active control of MHD instabilities, composed of 192 saddle coils, independently fed, arranged into a 48×4 grid housed inside a stainless steel Toroidal Support Structure (TSS) and a wide set of magnetic sensors (192 bi-axial pick-up probes measuring toroidal and poloidal B components and 192 saddle sensors for the radial component) [3].

The successful simultaneous feedback control of a spectrum of MHD instabilities has allowed to reach the design plasma current of 2 MA in the RFP configuration [4] and to operate stationary tokamak discharges with $q(a) < 2$, by controlling the $m = 2$, $n = 1$ RWM [5].

In order to bring the plasma closer to the shell w.r.t. RFX-mod and consequently reduce the error field at the edge, an upgrade is presently under investigation (more details on scientific and technological aspects can be found in [6,7]): the main foreseen mechanical modifications are the removal of the Vacuum Vessel (VV), the realisation of a new vacuum boundary on the TSS and the introduction of a new butt joint gap configuration (both shell and TSS) in order to allow the machine assembling. In this paper we focus on the electromagnetic analysis of the MHD control system in RFX-mod upgrade (hereafter RFX-mod2) with particular

* Corresponding author at: Consorzio RFX, C.so Stati Uniti 4, 35127 Padova, Italy.
E-mail address: paolo.bettini@unipd.it (P. Bettini).

http://dx.doi.org/10.1016/j.fusengdes.2017.02.094
0920-3796/

emphasis on the frequency response of the copper shell. If not carefully addressed, this problem may easily lead to unfeasible memory and computational time requirements. Therefore, a state of the art integral formulation, coupled to the sparsification procedure summarised in Section 3, is used to solve the eddy current problem in the frequency domain. Initial numeric results are presented in Section 4.

2. Integral formulation

RFX-mod2 copper shell has a thickness (δ = 3 mm) much smaller than the penetration depth of the magnetic field at the highest frequency of interest (50 Hz). Thus, the induced current density can be considered as uniform across the layer thickness and a surface integral approach can be adopted, as described in the following. Additional details may be found in [8].

The surface representing the thin conductor is meshed with a triangular mesh formed by N nodes $\{N_i\}_{i=1}^N$, E edges $\{E_j\}_{j=1}^E$ and T triangles $\{T_k\}_{k=1}^P$. From the mesh, the primal cell complex $\mathcal{K}$ [9] is constructed as follows, see Fig. 1a. The elements are defined as rectangular prisms $\{v_i\}_{i=1}^P$ constructed by considering the polygons with a thickness δ. Faces $\{f_i\}_{i=1}^E$ are defined as the lateral faces of the prisms (one-to-one with the mesh edges), and edges $\{e_i\}_{i=1}^N$ are those normal to the symmetry plane (one-to-one with the mesh nodes). We remark that these prisms of thickness δ are used only to explain the formulation but they are not explicitly constructed in the implementation. Then, the dual nodes $\tilde{n}$, dual edges $\tilde{e}$ and dual faces $\tilde{f}$ belonging to the dual complex $\tilde{\mathcal{K}}$ are constructed. They are obtained from $\mathcal{K}$ with the standard *barycentric subdivision* [9], see Fig. 1b. Interconnections of the geometric elements of the primal and dual complex are given in terms of usual incidence matrices. We consider the incidence matrices $\mathbf{C}$ between pairs (f, e) and $\tilde{\mathbf{C}}$ between pairs $(\tilde{f}, \tilde{e})$, in regard to which $\tilde{\mathbf{C}} = \mathbf{C}^T$ holds [9], and the incidence matrix $\mathbf{D}$ between pairs (v, f).

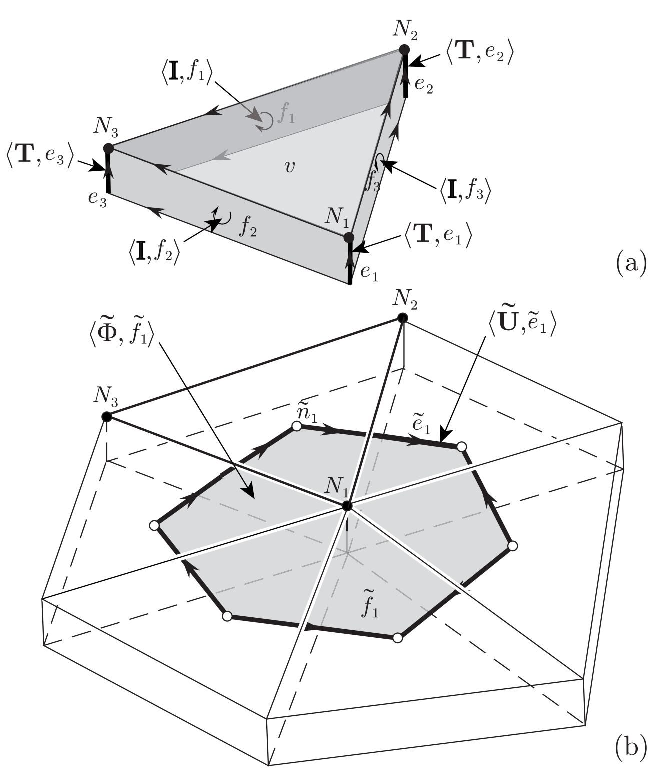

Fig. 1. Association of physical variables to geometric elements of the (a) primal and (b) dual complexes.

We associate an unknown current on faces $f_i \in \mathcal{K} - \partial\mathcal{K}$, whereas we assume that the current is zero on boundary faces to prevent current flowing outside the thin conductor. Such unknown currents are stored in the array $\mathbf{I}$, one entry I_i for each face f_i. Since $\mathbf{I}$ is solenoidal (i.e. $\mathbf{DI} = \mathbf{0}$) it can be represented by

$$\mathbf{I} = \mathbf{CT} + \mathbf{Hi}, \tag{1}$$

where $\mathbf{T}$ is the array containing the circulations of the electric vector potential on mesh edges, $\mathbf{i}$ is the array of *independent currents* [10]; the columns of $\mathbf{H}$ store the representatives of $H^2(\mathcal{K} - \partial\mathcal{K})$ generators. An introduction to algebraic topology, comprising the definition of cohomology generators, can be found in [10–12].

Concerning boundary conditions, the coefficients of $\mathbf{T}$ on edges on $\partial\mathcal{K}$ should be set to zero. Moreover, if some connected components of $\mathcal{K}$ is closed, i.e. without boundary, $\mathbf{T}$ on one arbitrary edge of each of such connected components has to be fixed to zero. Then, the discrete Faraday's law is enforced on the boundary of dual faces that are dual to interior edges

$$\mathbf{C}^T\mathrm{U} + i\omega\Phi = -i\omega\mathbf{C}^T\tilde{\mathbf{A}}_s, \tag{2}$$

where U is the electromotive force (e.m.f.) on dual edges, Φ is the magnetic flux produced by eddy currents through dual faces and $\tilde{\mathbf{A}}_s$ is the circulation of the magnetic vector potential due to the source currents on dual edges. Standard discrete constitutive laws read as

$$\mathrm{U} = \mathbf{RI} \quad \text{and} \quad \mathrm{A} = \mathbf{MI}, \tag{3}$$

where $\mathbf{R}$ and $\mathbf{M}$ are the classical resistance mass matrix and the magnetic matrix [13], respectively. By substituting (1), (3) and $\Phi = \mathbf{C}^T\mathrm{A}$ inside (2) and by defining $\mathbf{K} = \mathbf{R} + i\omega\mathbf{M}$,

$$\left(\mathbf{C}^T\mathbf{KC}\right)\mathbf{\Psi} + \left(\mathbf{C}^T\mathbf{KH}\right)\mathbf{i} = -i\omega\mathbf{C}^T\tilde{\mathbf{A}}_s. \tag{4}$$

The boundaries of dual faces is where discrete Faraday's laws as (2) are enforced. Then, Faraday's law holds also for any linear combination of those boundaries. Yet, e.m.f.s evaluated on loops that do not bound are still undetermined since they cannot be spanned by a linear combination of dual faces boundaries. Hence, non-local Faraday's laws enforced on suitable cycles have to be added

$$\left(\mathbf{H}^T\mathbf{KC}\right)\mathbf{T} + \left(\mathbf{H}^T\mathbf{KH}\right)\mathbf{i} = -i\omega\mathbf{H}^T\tilde{\mathbf{A}}_s. \tag{5}$$

3. Sparsification

The sparsification of the dense blocks of the linear system is obtained by means of hierarchical $\mathcal{H}$-matrices obtained with Adaptive Cross Approximation (ACA). The main features of this approach are summarised in the following. Additional details may be found in [16].

The implementation has been achieved through the *hlibpro* library [19], which allows the parallel construction of the matrix and the solution of the resulting linear system of equations, with only small, localised modifications to the existing non-sparsified code. The method works by partitioning and clustering the degrees of freedom according to a geometrical criterion. Then each cluster pair is tested against an admissibility criterion. If the cluster pair satisfies the criterion, the corresponding matrix block belongs to the far-field, otherwise the clusters are halved and the procedure is applied recursively until the number of elements is larger than a specified threshold. The near-field submatrices are computed exactly, whereas the far-field ones are approximated with ACA, obtaining a low rank approximation $\tilde{\mathbf{W}}_k$ of the far-field interaction matrix $\mathbf{W}$ in $\mathbb{R}^{m\times n}$, such that

$$\|\tilde{\mathbf{W}} - \tilde{\mathbf{W}}_k\|_F \le \epsilon\|\tilde{\mathbf{W}}\|_F, \tag{6}$$

where $k < m, n, \epsilon$ is a specified accuracy and $\|\cdot\|_F$ the Frobenius norm. The low rank approximation can be obtained without the explicit construction of $\tilde{\mathbf{W}}$ [18] by choosing a subset of rows and column such that

$$\tilde{\mathbf{W}}_k = \mathbf{U}\mathbf{V}^{\mathrm{T}}, \quad \mathbf{U} \in \mathbb{R}^{m\times k}, \quad \mathbf{V} \in \mathbb{R}^{n\times k}. \tag{7}$$

Since only a few entries of the original matrix must be computed, it can be shown that the computational and memory cost of this technique have linear-logarithmic complexity [17]. $\mathcal{H}$-matrix arithmetics is also used to construct an incomplete LU decomposition which is used as preconditioner for the GMRES solver. The low rank approximation of the system matrix of the case presented in Section 4 is built in 720 s using the ACA+ algorithm [19]; the compression ratio is ≈5.8% (3.6 GB compared to 62.5 GB). The preconditioned system converged to the solution in ≈150 s using GMRES on a Intel(*R*) Xeon(*R*) double E5-2680 (2.7 GHz).

4. Numerical results

A detailed 3D electromagnetic model of RFX-mod2 has been developed, which includes the copper shell, 192 actuators and a 720 × 180 grid of synthetic sensors (three-axial field measures) distributed on a toroidal surface (first wall, $R_0 = 1.995$, $a = 0.489$ m). The shell (see Fig. 2) features one toroidal gap on the equatorial plane ($\theta = 0°$) and the following local (non-axisymmetric) elements:

- 2 poloidal gaps 180° degrees apart,
- 80 ports for diagnostics, vacuum, heating systems.

In order to quantify the distortion of the magnetic field generated by the MHD saddle coils [15], due to the non-homogeneous features of the copper shell, a simulation has been performed by feeding the coils with a set of independent currents to produce in vacuum (i.e. without conducting structures) an harmonic pattern as follows: the current for the i, j coil ($i = 1, \ldots, 48$, $j = 1, \ldots, 4$) is described by $I_0 sin(n\phi_{c,i} - \Phi_j + 2\pi f t)$ where I_0 is the oscillation amplitude, $\phi_{c,i}$ is the toroidal angle of the ith coil and the initial phase $\Phi_j = m\, j\pi/2$ varies according to the poloidal coil index. In the following, an $m = 1$, $n = 6$ pattern is considered which is expected to correspond to the innermost resonant tearing mode of RFX-mod2. The simulation is performed at $f = 20$ Hz, which is in the range of the experimentally observed rotation of Tearing Modes in RFX-mod [5]. Fig. 3 shows the 3D current density pattern on RFX-mod2 shell with such an harmonic excitation.

Fig. 4-top shows the map of the total (coils + structures) radial field at the plasma radius, at a given time during the oscillation period. Along the toroidal and poloidal gaps the radial field (B_r) oscillation amplitude is significantly bigger than the homogeneous

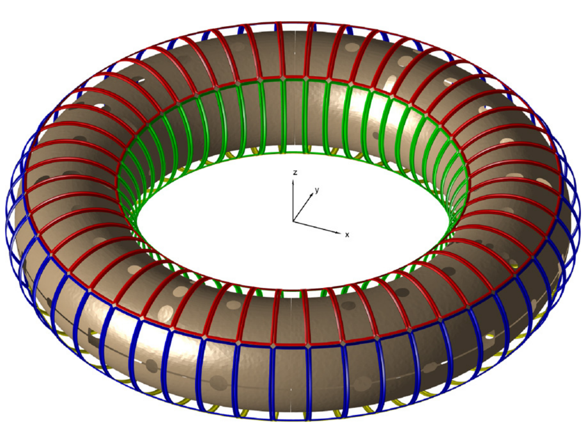

Fig. 2. 3D electromagnetic model of RFX-mod2. The shell is discretised with 131,547 triangles, 67,493 nodes and 199,118 edges.

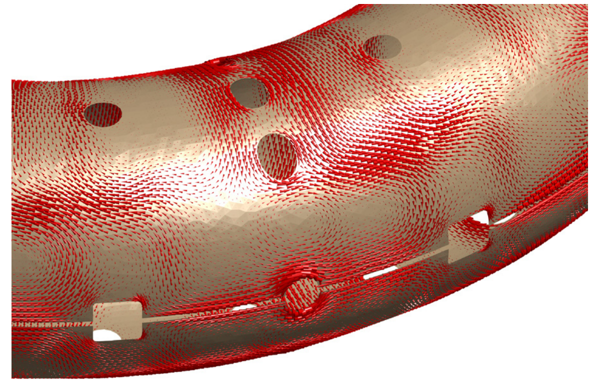

Fig. 3. Real part of the current density on RFX-mod2 shell with harmonic excitation ($m = 1$, $n = 6$, $f = 20$ Hz).

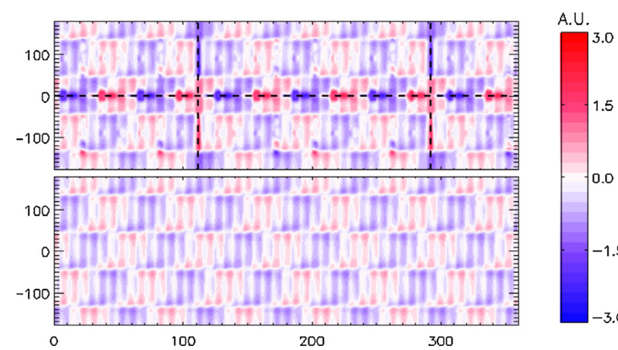

Fig. 4. Top: map of the radial field at a given time. Dashed lines correspond to toroidal and poloidal gaps. Bottom: radial field for a continuous and homogeneous torus.

torus case (4-bottom). The amplification (or suppression) map of radial field is shown in Fig. 5: along the poloidal and toroidal gap the radial field is greatly amplified while in regions of portholes a bipolar structure occurs. The asymmetry between the two sides of the portholes is due to the direction of rotation of the $n = 6$ pattern. The phase of the radial field oscillation is significantly modified too.

This pattern of amplification and phase delays has important consequences on the spectrum of the magnetic field. Given the finite size of the coils, the poloidal and toroidal spectrum is characterised by the presence of infinite sidebands $m = 1 + kM$, $n = 6 + hN$: the black line of Fig. 6-left shows the m sidebands of the $m = 1$, $n = 6$ harmonic. The amplitude of the main harmonic is reduced by an amount which is consistent with the one that can be computed in

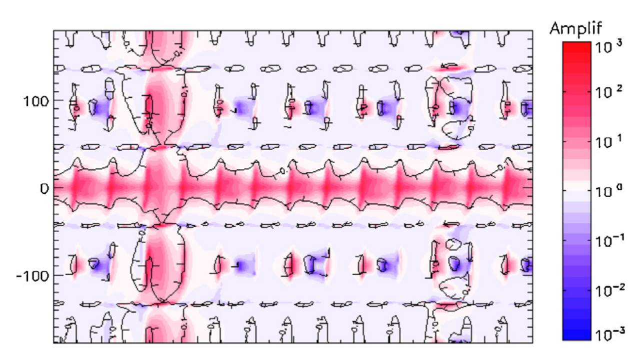

Fig. 5. Amplification (or suppression) map of radial field. The continuous line encloses a region where the phase delay w.r.t. the homogeneous torus case is above 0.1π (and up to 0.5π).

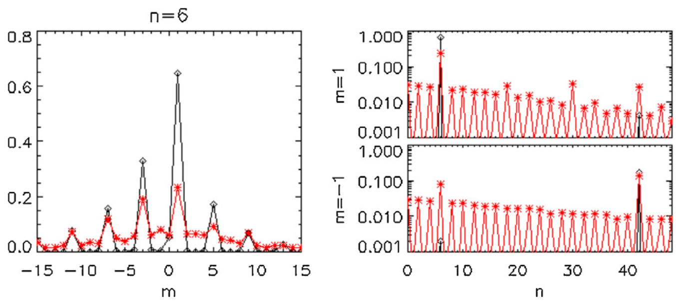

Fig. 6. Poloidal (left) and toroidal (right) spectrum of the radial magnetic field. The harmonics due to the presence of the shell (red line) are compared to the DC case (black line). (For interpretation of the references to color in this figure legend, the reader is referred to the web version of this article.)

the cylindrical approximation. The significant enhancement of the radial field in the region localised at the toroidal gap at $f = 20$ Hz generates a broad continuum spectrum of harmonics (red line). On the other hand, the effect on the n spectrum of the gaps and port holes is twofold: on one hand the two gaps generate a significant amount of even harmonics, while the ports are responsible for the enhancements of selected harmonics, such as $m = 1$, $n = 18$ and $m = 1$, $n = 30$.

5. Conclusions

An efficient and fast computation technique has been developed to compute the dynamics of the magnetic field generated by the saddle coils of the RFX-mod control system as modified by the presence of an unhomogeneous copper shell. The model can easily simulate the measurements of the pick-up probes of both RFX-mod and the proposed RFX-mod2. The former application will help developing a more accurated de-aliasing algorithm [20] for analysing experiments performed in the past, while the latter will guide the design of new sensors for RFX-mod2 and a new de-aliasing algorithm.

Acknowledgments

The authors would like to thank Marco Bernardi for his valuable CAD design work.

References

[1] R. Piovan, et al., RFX machine and power supply improvements for RFP advanced studies, Fusion Eng. Des. 56–57 (2001) 819–824.
[2] P. Martin, et al., New insights into MHD dynamics of magnetically confined plasmas from experiments in RFX, Nucl. Fusion 42 (2002) 247–257.
[3] P. Sonato, et al., Machine modification for active MHD control of RFX, Fusion Eng. Des. 66–68 (2003) 161–168.
[4] P. Martin, et al., Nucl. Fusion 51 (2011) 094023.
[5] P. Zanca, et al., Advanced feedback control of MHD instabilities: comparison of compensation techniques for radial sensors, Plasma Phys. Contr. Fusion 5 (2012) 124018.
[6] M. Zuin, et al., Overview of the RFX-mod Fusion Science Activity, Nuclear Fusion, Special Issue, “IAEA Fusion Energy Conference”, 2017.
[7] S. Peruzzo, et al., Design concept of machine upgrades for the RFX-mod experiment, Fusion Engineering and Design, Special Issue, “Proceedings SOFT 2016”, 2017.
[8] P. Bettini, P. Dłotko, R. Specogna, A boundary integral method for computing eddy currents in non-manifold thin conductors, IEEE Trans. Magn. 52 (3) (2016) 7203104.
[9] E. Tonti, A direct discrete formulation of field laws: the cell method, CMES 2 (2001) 237–258.
[10] P. Dłotko, R. Specogna, Cohomology in 3D magneto-quasistatics modeling, Commun. Comput. Phys. 14 (1) (2013) 46–76.
[11] P. Bettini, R. Specogna, A boundary integral method for computing eddy currents in thin conductors of arbitrary topology, IEEE Trans. Magn. 51 (3) (2015) 7203904.
[12] J.R. Munkres, Elements of Algebraic Topology, Perseus Books, New York, 1984.
[13] A. Kameari, Transient eddy current analysis on thin conductors with arbitrary connections and shapes, J. Comput. Phys. 42 (1981) 124–140.
[15] P. Bettini, L. Marrelli, R. Specogna, Calculation of 3-D magnetic fields produced by MHD active control systems in fusion devices, IEEE Trans. Magn. (50) (2014) 7000904.
[16] P. Alotto, P. Bettini, R. Specogna, Sparsification of BEM matrices for large-scale eddy current problems, IEEE Trans. Magn. 52 (3) (2016), art. no. 7203204.
[17] M. Bebendorf, Hierarchical Matrices, Ser. Lecture Notes in Computational Science and Engineering, Springer Verlag, 2008.
[18] S. Kurz, O. Rain, S. Rjasanow, The adaptive cross-approximation technique for the 3-D boundary-element method, IEEE Trans. Magn. 38 (2) (2002) 421–424.
[19] R. Kriemann, HLIBpro. http://www.hlibpro.com.
[20] L. Marrelli, et al., Plasma Phys. Contr. Fus. 49 (2007) B359.